The Generation of Surfzone Eddies in a Strong Alongshore Current

FALK FEDDERSEN

Scripps Institution of Oceanography, La Jolla, California

(Manuscript received 4 March 2013, in final form 19 October 2013)

ABSTRACT

The surfzone contains energetic two-dimensional horizontal eddies with length scale larger than the water depth. Yet, the dominant eddy generation mechanism is not understood. The wave-resolving model funwaveC is used to simulate surfzone eddies in four case examples, from the SandyDuck field experiment, that had alongshore uniform bathymetry. The funwaveC model is initialized with the observed bathymetry and the incident wave field in 8-m depth and reproduces the observed cross-shore structure of significant wave height and mean alongshore current. Within the surfzone, the wave-resolving funwaveC-modeled $E(f, k_y)$ spectra and the bulk (frequency and k_y integrated) rotational velocities are consistent with the observations below the sea–swell band (<0.05 Hz), demonstrating that the model can be used to diagnose surfzone eddy generation mechanisms. In the mean-squared perturbation vorticity budget, the breaking wave vorticity forcing term is orders of magnitude larger than the shear instability generation term. Thus, surfzone eddies (vorticity) generally are not generated through a shear instability, with possible exceptions for very narrow banded in frequency and direction and highly obliquely large incident waves. The alongshore wavenumber spectra of breaking wave vorticity forcing is broad with the majority (>80%) of vorticity forcing occurring at short alongshore scales <20 m. However, the alongshore wavenumber spectra of vorticity is red, which may be due to a 2D turbulence inverse energy cascade bringing energy to longer wavelengths or may result from an amplified vorticity response to direct forcing at smaller k_y.

1. Introduction

The surfzone is a place of energetic two-dimensional (2D) horizontal turbulent eddies with length scales greater than the water depth. These horizontal eddies (hereafter termed eddies) have rotational (as opposed to irrotational) velocities associated with vertical vorticity (hereafter termed vorticity). Recent observations and modeling indicate that absolute cross-shore diffusivity, inferred from dye tracers on an alongshore uniform beach, is related to the bulk (surfzone averaged) root-mean-square (rms) horizontal rotational velocities associated with eddies (Clark et al. 2010, 2011). Drifter-derived time-dependent absolute cross-shore diffusivities were consistent with stirring due to surfzone eddies with Lagrangian (not Eulerian) time scales of $O(100\,\text{s})$ (Spydell and Feddersen 2012b). When alongshore current shear was strong, drifter-derived alongshore diffusivities were well predicted by a shear dispersion theory that includes nonzero Lagrangian time scale (Spydell and Feddersen 2012a). Thus, 2D surfzone eddies are responsible for dispersion and dilution of surfzone tracers on alongshore uniform beaches. On rip-channeled (not alongshore uniform) beaches, dispersion may occur owing to both 2D eddies and mean circulation features (e.g., Brown et al. 2009).

The most commonly considered (nonpassive) surfzone tracer is sediment. Yet, tracers can also include bubbles (Ma et al. 2011) and pathogens (e.g., Rippy et al. 2013; Feng et al. 2013) that impose health risk on bathers (e.g., Haile et al. 1999). Gametes and larvae of invertebrates that live in the beach face (such as *Donax* clams) are also influenced by the stirring of 2D surfzone eddies as they traverse the surfzone. Understanding the processes that generate 2D surfzone eddies is critical to improved understanding of surfzone tracer dispersion.

Time-dependent 2D eddies within the surfzone were first identified as a low frequency, nondispersive ridge in frequency f and alongshore wavenumber k_y velocity spectra $E(f, k_y)$ outside of the gravity wave region (Oltman-Shay et al. 1989). These motions have variability on Eulerian time scales between 50 and 500 s

Corresponding author address: F. Feddersen, SIO, 9500 Gilman Dr., La Jolla, CA 92093-0209.
E-mail: falk@coast.ucsd.edu

DOI: 10.1175/JPO-D-13-051.1

and alongshore length scales between 40 and 250 m, and $E(f, k_y)$ ridge slopes are approximately equal to the mean alongshore current V (e.g., Oltman-Shay et al. 1989; Noyes et al. 2004). The magnitude of these eddy velocities was also generally related to V (Noyes et al. 2004). However, even during times of weak V, surfzone eddies are observed. For example, on a monotonic, alongshore uniform beach with $V = 0\,\mathrm{m\,s^{-1}}$, the presence of a scale-dependent relative diffusivity indicated the presence of an energetic eddy field with scales varying from 10 to 50 m (Spydell et al. 2007; Spydell and Feddersen 2009). During times of weak $|V|$ ($<0.25\,\mathrm{m\,s^{-1}}$), eddies (rotational velocity outside of the gravity wave region) were observed with eddy velocities of 0.1–0.2 $\mathrm{m\,s^{-1}}$, which increased linearly with increased wave height (MacMahan et al. 2010).

With linear stability analysis, the motions associated with the $E(f, k_y)$ ridge were associated with the shear instability of the alongshore current (e.g., Bowen and Holman 1989; Dodd et al. 1992; and many others), which is an intrinsic eddy generation mechanism. Thus, these motions were subsequently dubbed ''shear waves.'' Shear instabilities of the mean alongshore current, in particular their nonlinear equilibration, have been studied with a nonlinear shallow-water equation (NSWE) with steady wave forcing (thus only allowing the intrinsic eddy generation) both numerically (e.g., Allen et al. 1996; Slinn et al. 1998; Özkan-Haller and Kirby 1999; Noyes et al. 2005) and analytically (Feddersen 1998). NSWE model-derived $E(f, k_y)$ reproduced the overall ridge slope of the observed $E(f, k_y)$ (Özkan-Haller and Kirby 1999; Noyes et al. 2005). However, the model energy generally is concentrated at lower f–k_y than observed, at any k_y is less broad in frequency than observed, and often underpredicts the overall variance (Noyes et al. 2005).

Vorticity associated with 2D surfzone eddies is also generated through the extrinsic mechanism of breaking wave vorticity forcing, which can occur at a range of alongshore length scales from 10 to 100+ m. Typically, breaking wave vorticity forcing is conceptualized through two mechanisms: short-crested wave breaking and wave groups. Short-crested breaking wave vorticity forcing is due to along-crest variation in wave dissipation (Peregrine 1998). Recently, changes in vorticity with the passage of individual short-crested breaking waves was observed at 10+ m length scales (Clark et al. 2012), consistent with the theory of Peregrine (1998). Wave-resolving (WR) models, such as Boussinesq models (e.g., Chen et al. 2003; Feddersen et al. 2011), can generate vorticity by this mechanism. On alongshore uniform beaches, such along-crest variation requires the presence of obliquely incident waves, whether obliquely incident monochromatic waves or random, directionally spread waves. Using a WR Boussinesq model on a case with highly obliquely incident waves (35° in 8-m depth), Chen et al. (2003) found 1.5 times larger rms surfzone vorticity with monochromatic unidirectional waves relative to directionally spread random waves. However, the vorticity generation mechanisms (shear instability versus wave forcing) were not discussed nor were the length scale of the vorticity forcing or resulting vorticity examined. For alongshore uniform beaches and random waves with a zero mean wave angle, wave directional spread (Kuik et al. 1988) is required to generate vorticity. For constant incident wave energy and normally incident mean wave angle, modeled surfzone-averaged rms vorticity increases with increasing wave directional spread (Spydell and Feddersen 2009). Because V was essentially zero, the rms vorticity was generated by breaking wave vorticity forcing (Spydell and Feddersen 2009).

Because the length scale of horizontal surfzone eddies is much larger than the water depth, the dynamics of surfzone eddies likely follow those of forced and dissipative 2D turbulence (e.g., Kraichnan and Montgomery 1980; Tabeling 2002; Boffetta and Ecke 2012). A basic principle of (both freely decaying and forced) 2D turbulence is that eddy energy cascades to longer length scales through nonlinear interactions. Therefore, vorticity injected at short scales of 10+ m may evolve to larger length scales, creating a rich wavenumber spectrum of surfzone eddies.

Surfzone vorticity can also be generated at the longer alongshore length scales of wave groups, which are related to the k_y width (Δk_y) of the incident wave field. Although this mechanism is also present in WR models, it is more commonly associated with wave-averaged (WA) models where the vorticity forcing is due to the alongshore variation of (wave breaking induced) radiation stress gradients associated with wave groups: the slow time and slow alongshore evolution of the wave envelope (e.g., Reniers et al. 2004; Long and Özkan-Haller 2009). Wave groups are typically modeled with a wave action equation, which requires (e.g., Van Dongeren et al. 2003; Reniers et al. 2004) that the incident wave spectra must have small frequency spread ($\Delta f/f_p \ll 1$), where f_p is the peak frequency, and small directional spread σ_θ. These limitations imply that the vorticity forcing induced by groups must be at much larger length scales than that of short-crested breaking wave vorticity forcing. On alongshore uniform beaches, WA models with wave group forcing can generate very low-frequency (VLF < 0.004 Hz) rotational motions that have alongshore length scales $\sim$100 m or longer (Reniers et al. 2004). A WA model with wave group forcing (Long and Özkan-Haller 2009) also gave a broader $E(f, k_y)$ spectrum than intrinsic (shear instability only)

models (Noyes et al. 2005). WA models with wave group forcing have been successful in reproducing VLF eddy velocities on rip-channeled beaches (Reniers et al. 2007, 2009). When $V \approx 0\,\mathrm{m\,s^{-1}}$ (implying $dV/dx \approx 0\,\mathrm{s^{-1}}$) and a shear instability is not possible, modeled surfzone VLF eddy velocities, simulated with a linear (WA) wave group model, agreed with observations within a factor of 2 (MacMahan et al. 2010). Linear and nonlinear WA model solutions were similar, with nonlinear solutions more broad in k_y space, particularly at larger k_y (MacMahan et al. 2010). However, as 2D turbulence cascades eddy energy to longer length scales, it is unclear how wave-group-forced motions would generate eddies at the shorter 5–50-m scales noted in drifter two-particle observational (Spydell et al. 2007) and modeling (Spydell and Feddersen 2009) studies.

Whether shear instabilities or vorticity generated by wave breaking is the more important term in generating surfzone eddies remains an open question. In addition, the relative importance of short crested [$O(10\,\mathrm{m})$ scales] versus wave group (at much longer scales) vorticity forcing in generating surfzone eddies is not well understood. For an idealized surfzone with an alongshore current $\sim 0.5\,\mathrm{m\,s^{-1}}$ strong enough to be unstable, Long and Özkan-Haller (2009) found that vorticity generated by shear instabilities and by wave group forcing contributed approximately equally to surfzone-averaged squared potential vorticity dynamics. However, the shorter scales of vorticity injection by individual breaking waves were not included, and the model was not compared to field observations. Observations of surfzone eddies with strong V have not been directly compared to a model that includes both the intrinsic shear instability mechanism and extrinsic wave forcing (short crested or wave groups) mechanisms.

Here, the WR Boussinesq model funwaveC is used to diagnose the relative importance of the intrinsic shear instability mechanism and the extrinsic (short crested or wave group) wave breaking mechanism in generating surfzone eddies. Four case examples from the SandyDuck field experiment, where observed $E(f, k_y)$ spectra were compared to results from a NSWE model with steady forcing (Noyes et al. 2005), are simulated with funwaveC. The funwaveC model is initialized with the observed bathymetry and incident directional wave field in 8-m water depth (section 3). The funwaveC model predicts well the cross-shore variation in significant wave height H_s and mean alongshore current V (section 4a). For these four cases, within the surfzone the funwaveC-modeled $E(f, k_y)$ spectra (section 4b) and the bulk (frequency and k_y integrated) rotational velocities (section 4c) are consistent with the observations, demonstrating that eddy dynamics can be diagnosed with funwaveC. Vorticity dynamics are examined in section 5. The mean-squared perturbation vorticity budget is examined to determine the relative importance of shear instability and breaking wave vorticity forcing in generating surfzone eddies (section 5a). The alongshore wavenumber spectra of breaking wave vorticity forcing and vorticity are examined to explore the dominant-forcing alongshore length scales and the induced vorticity response (section 5b). The results are discussed in section 6 and summarized in section 7.

2. Surfzone observations

Observations were collected as part of the SandyDuck experiment in August–November 1997 at the Army Corps of Engineers Field Research Facility (FRF) in Duck, North Carolina. The observations are described in detail elsewhere (Elgar et al. 2001; Feddersen and Guza 2003; Noyes et al. 2002, 2004) and are briefly discussed here. The FRF coordinate system is used where x is the cross-shore coordinate increasing offshore with the shoreline near $x = 110\,\mathrm{m}$ and y is the alongshore coordinate. A dense cross-shore array of collocated pressure gauges and current meters (PUV) were deployed at 11 locations on a cross-shore transect extending from the shoreline to 5.5-m water depth to measure cross-shore wave and current transformation. In addition, five alongshore arrays (denoted A1–A5 from closest to farthest from shore) of PUV were deployed (Fig. 1) to measure $E(f, k_y)$ for both cross-shore u and alongshore v velocities using an iterative maximum likelihood estimator at frequencies below the sea–swell band ($<0.05\,\mathrm{Hz}$) (Noyes et al. 2002, 2004). A pressure sensor array in 8-m water depth provides incident wave statistics including wave spectra, mean wave angle $\overline{\theta}(f)$, and directional spread $\sigma_\theta(f)$ (Kuik et al. 1988). Wind stress τ_w was estimated from measurements at the end of the FRF pier. Observations of surfzone eddies during the 4-month-long SandyDuck experiment are described by Noyes et al. (2004) and MacMahan et al. (2010). Using a NSWE model with steady forcing, Noyes et al. (2005) simulated four, 3-h-long case examples, 28 August (0828), 1 November (1101), 13 November (1113), and 17 November (1117), that are also simulated here. The bathymetry and mean circulation in the instrumented area usually was alongshore homogeneous (Feddersen and Guza 2003), although alongshore variability of V at the shallowest array A1 was significant on 1101 and 1113.

3. Models

a. Wave-resolving model funwaveC

The open-source wave-resolving Boussinesq model funwaveC has been previously used to study a variety of

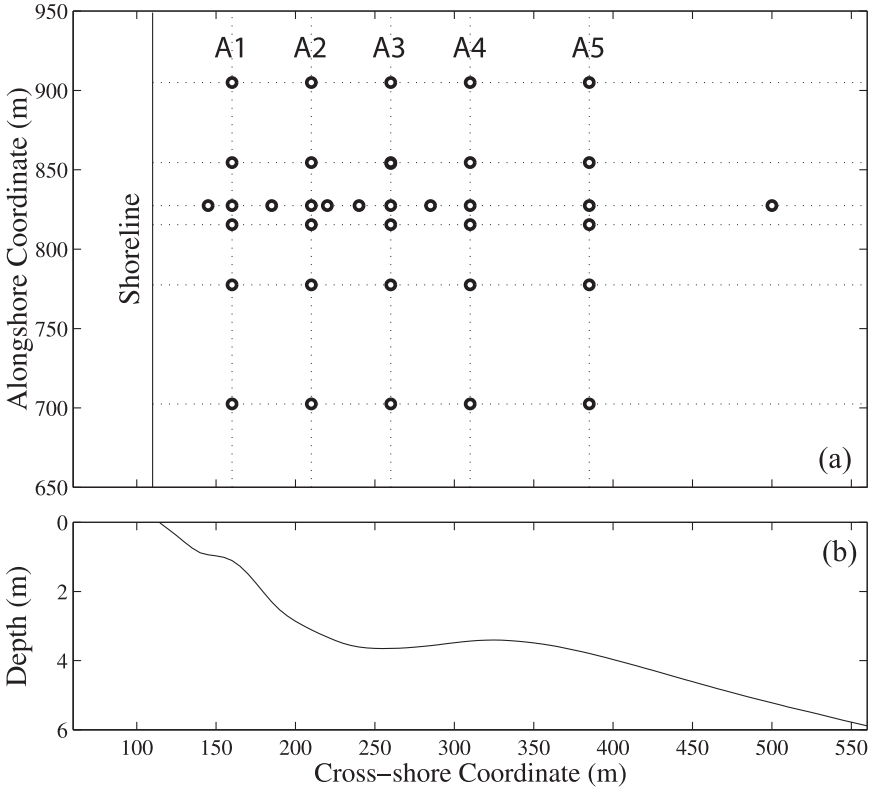

FIG. 1. (a) Plan view of SandyDuck instrument array. Each circle indicates a velocity sensor. The FRF coordinate system is used where (x, y) are cross- and alongshore, respectively. The five alongshore arrays are indicated A1–A5. The approximate location of the shoreline is near $x = 110$ m. (b) Alongshore-averaged depth below mean sea level vs cross-shore coordinate.

surfzone processes including cross-shore tracer dispersion driven by individual bores (Feddersen 2007), surfzone drifter dispersion in a weak alongshore current (Spydell and Feddersen 2009), spectral wave transformation, mean currents, and surfzone eddies (Feddersen et al. 2011), cross-shore tracer dispersion in moderate alongshore currents (Clark et al. 2011), shoreline runup (Guza and Feddersen 2012), and net circulation cells on coral reef spur and groove formations (Rogers et al. 2013). The model is briefly described here. Additional details are found elsewhere (Feddersen et al. 2011).

The time-dependent Boussinesq funwaveC model equations of Nwogu (1993) are similar to the nonlinear shallow-water equations but include higher order dispersive terms. The mass conservation equation is

$$\frac{\partial \eta}{\partial t} + \nabla \cdot [(h+\eta)\mathbf{u}] + \nabla \cdot \mathbf{M}_d = 0,$$

where η is the instantaneous free-surface elevation, t is time, h the still water depth, $\mathbf{u}$ the instantaneous horizontal velocity at the reference depth $z_r = -0.531h$ (where $z = 0$ at the still water surface), and $\mathbf{M}_d$ is the dispersive term (Nwogu 1993). The two-dimensional horizontal gradient operator ∇ operates on the cross-shore x and alongshore y directions. The momentum equation is

$$\frac{\partial \mathbf{u}}{\partial t} + \mathbf{u} \cdot \nabla \mathbf{u} = -g\nabla\eta + \mathbf{F}_d + \mathbf{F}_{\mathrm{br}} - \frac{\boldsymbol{\tau}_b}{(\eta+h)} + \frac{\boldsymbol{\tau}_w}{(\eta+h)} - \nu_{\mathrm{bi}}\nabla^4\mathbf{u}, \quad (1)$$

where g is gravity, $\mathbf{F}_d$ the dispersive term (Nwogu 1993), $\mathbf{F}_{\mathrm{br}}$ the breaking term, $\boldsymbol{\tau}_b$ is the instantaneous bottom stress, and $\boldsymbol{\tau}_w$ the surface (wind) stress. The biharmonic friction ($\nabla^4\mathbf{u}$) term damps instabilities with hyperviscosity ν_{bi} between 0.2 to 0.3 $\mathrm{m^4\,s^{-1}}$. The bottom stress is given by a quadratic drag law:

$$\boldsymbol{\tau}_b = c_d|\mathbf{u}|\mathbf{u}$$

with a nondimensional spatially constant drag coefficient c_d set between 2.3×10^{-3} and 2.6×10^{-3}, matching Noyes et al. (2005). Although observations

indicate a larger c_d within the surfzone relative to (typically 4–8-m depth) seaward of the surfzone (Feddersen et al. 1998), a cross-shore uniform c_d is used for simplicity and because a $c_d \approx 2.6 \times 10^{-3}$ is consistent with a cross-shore-integrated momentum balance between alongshore transects A1–A5 (Feddersen and Guza 2003).

During the four case examples, the observed weak alongshore wind stress is applied to the model. The effect of wave breaking on the momentum equations is parameterized as a Newtonian damping (Kennedy et al. 2000) where

$$\mathbf{F}_{\rm br} = (h+\eta)^{-1}\nabla\cdot[\nu_{\rm br}(h+\eta)\nabla\mathbf{u}].$$

The Lynett (2006) breaking wave eddy viscosity $\nu_{\rm br}$ parameterization is used here with standard parameters, as in Guza and Feddersen (2012).

The alongshore uniform model bathymetry is based on those used by Noyes et al. (2005) with an additional offshore 200-m-wide region of constant depth between 7 and 8 m and a subaerial beach extending to 2–2.4 m MSL, depending on the case example, to allow runup. The constant depth region contains the wavemaker and a 90-m offshore sponge layer that absorbs seaward-propagating waves. Shoreline runup is implemented using the ''thin layer'' method (Salmon 2002), as described in Guza and Feddersen (2012). The total cross-shore domain is near 870 m for all case examples. The cross- and alongshore grid sizes are 1 and 1.25 m, respectively. The alongshore domain width is 1500 m with alongshore periodic boundary conditions.

A wavemaker (Wei et al. 1999), located immediately onshore of the offshore sponge layer, generates a wave field that has a target frequency–directional spectrum based on the observed 8-m depth wave spectra $\overline{\theta}(f)$ and $\sigma_\theta(f)$. Aspects of the wavemaker are briefly described here with full details in Feddersen et al. (2011). Unlike the wave group model offshore boundary condition of a wave envelope (Van Dongeren et al. 2003), here wavemaker free-surface $\eta_{\rm WM}$ is directly forced (Wei et al. 1999) so that

$$\eta_{\rm WM} = \sum_i a_i \sum_j d_{ij}\cos(k_{y,ij}y - 2\pi f_i t - \chi_{ij}), \qquad (2)$$

where a_i is the amplitude at each frequency, d_{ij} is directional distribution, $k_{y,ij}$ the alongshore wavenumber, and χ_{ij} a uniformly distributed random phase. The amplitudes a_i are derived from the sea surface elevation spectrum. The frequency-dependent directional distribution d_{ij} is given by Gaussian distribution centered about $\overline{\theta}(f)$ with width related to $\sigma_\theta(f)$ that reproduces the observed directional spread (Feddersen et al. 2011).

The model wavemaker is forced at many randomly spaced discrete frequencies between $0.06 < f < 0.25$ Hz at an average frequency resolution of 0.0004 Hz. The randomly spaced frequencies make the wavemaker recurrence much longer than the model simulation. At the wavemaker, kh varied between 0.86 and 1.0 at the mean incident frequency [within the Nwogu (1993) limits] and a/h varied between 0.04 and 0.11 (on 1113). The realistic modeled incident directional wave field allows for vorticity generation at the short length scales of individual short-crested breaking waves and longer wave group scales. Note that the Boussinesq approximation requires that horizontal length scales are greater than the depth. With typical surfzone depths of <2.5 m, departures from the Boussinesq approximation might not be negligible for eddies with short length scales (<10 m).

For each case example, the model was run for 8000 s, and model output is analyzed over the last 5000 s. The 3000 s allowed for model spinup was sufficient for mean-square vorticity to equilibrate similar to other surfzone simulations (Feddersen et al. 2011). Modeled frequency-dependent wave spectral quantities and ''bulk'' sea–swell band wave quantities such as significant wave height H_s are calculated with the same estimation methods as the field observations (section 2). The mean alongshore current V is the time-averaged v. Note that the funwaveC model velocity in the surfzone is essentially vertically uniform, whereas the velocity observations were made at depths between 0.4 and 1.0 m above the bed (Feddersen and Guza 2003).

b. *Nonlinear shallow-water equation model*

The time-dependent, rigid-lid NSWE model with steady alongshore forcing used by Noyes et al. (2005) is also described briefly here. This model is similar to those used previously (e.g., Allen et al. 1996; Slinn et al. 1998). The model rigid-lid continuity equation is $\nabla\cdot(h\mathbf{u}) = 0$, and the momentum equation is similar to (1) with $\mathbf{F}_d$ and $\mathbf{F}_{\rm br}$ set to zero. This model averages over incident wave time scales and does not include wave–current interaction. The steady alongshore wave forcing is given by $F_y = -\rho^{-1}dS_{xy}/dx$, where S_{xy} is derived from a wave and roller transformation model [see Ruessink et al. (2001) for details] that best fits the wave observations (Noyes et al. 2005). The alongshore domain width was either 1000 or 1500 m with alongshore periodic boundary conditions. The model grid spacing was 2.5 m in both x and y. Full details can be found in Noyes et al. (2005).

4. Results: Model data comparison

a. *Significant wave height H_s and mean alongshore current V*

As a precondition to testing the model's ability to accurately simulate the surfzone eddy field, model data comparison is performed for bulk parameters such as

TABLE 1. Observed incident (8-m depth) wave parameters for the four SandyDuck case examples. In all cases, the energy-weighted frequency spread was between 0.04 and 0.05 Hz.

Date	f_p (Hz)	H_s (m)	$\lvert\overline{\theta}\rvert$	σ_θ
0828	0.12	0.78	14°	41°
1101	0.12	1.49	21°	54°
1113	0.13	2.70	11°	52°
1117	0.16	0.96	37°	45°

significant wave height H_s and mean alongshore current V. For the four case examples, the 8-m depth incident H_s varied between 0.78 and 2.70 m, and peak frequency f_p varied between 0.12 and 0.16 Hz (Table 1). In all four cases, the frequency spread varied between 0.04 and 0.05 Hz. The bulk (energy weighted) (Kuik et al. 1988) mean wave angle $|\overline{\theta}|$ varied between 11° and 37°, and the bulk directional spread σ_θ varied between 41° and 54° (Table 1). However, at any sea–swell frequency, the mean angle and directional spread were less than 25° and 30°, respectively. Note that these incident spectra are broader in frequency and direction than the analytical spectra used by Long and Özkan-Haller (2009) to derive their wave group envelope.

On 0828, the incident (8-m depth) $H_s = 0.78$ m, wave breaking begins between A1 and A2, and the model reproduces the observed cross-shore structure of H_s (Fig. 2a). The mean alongshore current V is near zero offshore of the surfzone, with surfzone maximum $|V| \approx 0.45\,\mathrm{m\,s^{-1}}$, and the cross-shore structure is well reproduced by the model (Fig. 2b). The model similarly reproduces the observed H_s (Figs. 2d,g,j) and V on the other three days (Figs. 2e,h,k). On 1101, the larger incident $H_s = 1.48$ m results in wave breaking just offshore of A2, driving a strong, narrow surfzone alongshore current jet with maximum $|V| \approx 1\,\mathrm{m\,s^{-1}}$. On 1113, the large incident $H_s = 2.70\,\mathrm{m\,s^{-1}}$ resulted in a wide surfzone that encompassed all five alongshore arrays (Fig. 2g) with broad relatively strong alongshore current ($|V| \geq 0.5\,\mathrm{m\,s^{-1}}$) at each (Fig. 2h). On 1117, incident $H_s = 0.96$ m with wave breaking just offshore of A2 (Fig. 2j), and the large incident wave angle drives relatively strong jetlike surfzone currents up to $|V| \approx 0.75\,\mathrm{m\,s^{-1}}$ (Fig. 2l). In contrast to the simple one-dimensional modeled $H_s(x)$ and $V(x)$ structure in Noyes et al. (2005), funwaveC model parameters were not tuned here to minimize model data error. The H_s is most poorly modeled on 1113, likely due to poorly known bathymetry as the morphology can evolve rapidly during large wave events.

b. *Frequency–alongshore wavenumber spectra $E(f, k_y)$*

Here, the funwaveC model-derived frequency–alongshore wavenumber spectra $E(f, k_y)$ of cross-shore velocity are compared to the observed $E(f, k_y)$ reported in Noyes et al. (2005) at alongshore arrays within and seaward of the surfzone. Recall that the funwaveC model generates eddies through both short-crested and wave

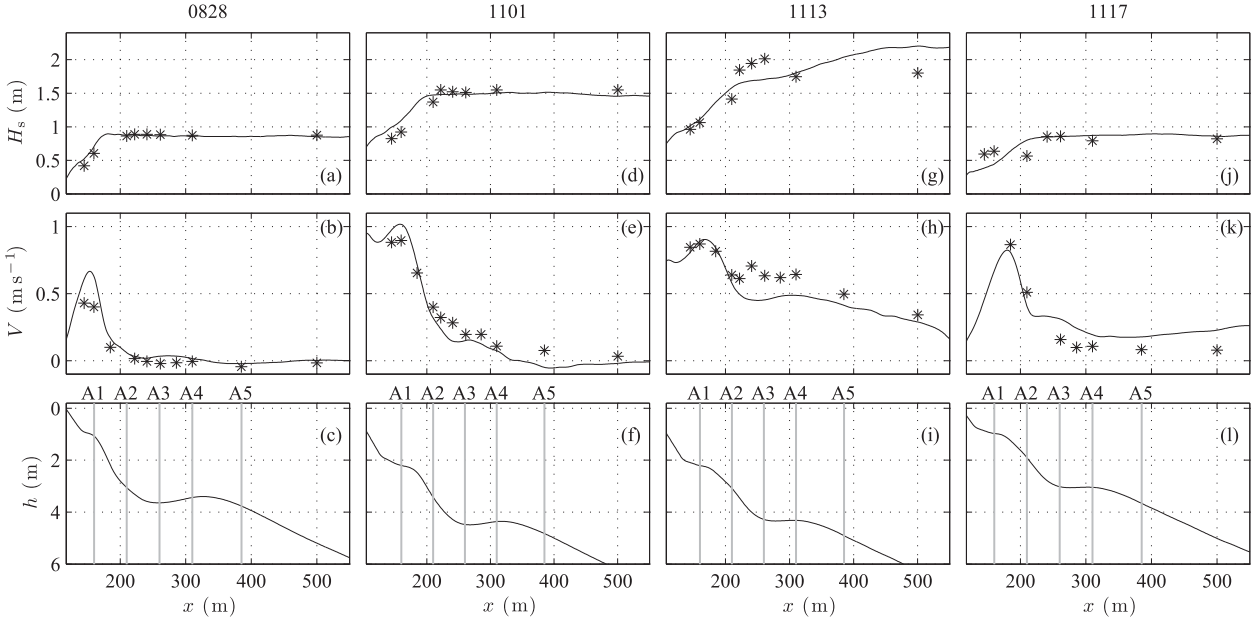

FIG. 2. (top) Modeled (funwaveC) and observed (symbols) significant wave height H_s curves, (middle) mean alongshore current V, and (bottom) depth h vs x in FRF coordinates for the four cases in Noyes et al. (2005) for (columns from left to right) 0828, 1101, 1113, and 1117. The shoreline location varies between $x = 107$ and 115 m.

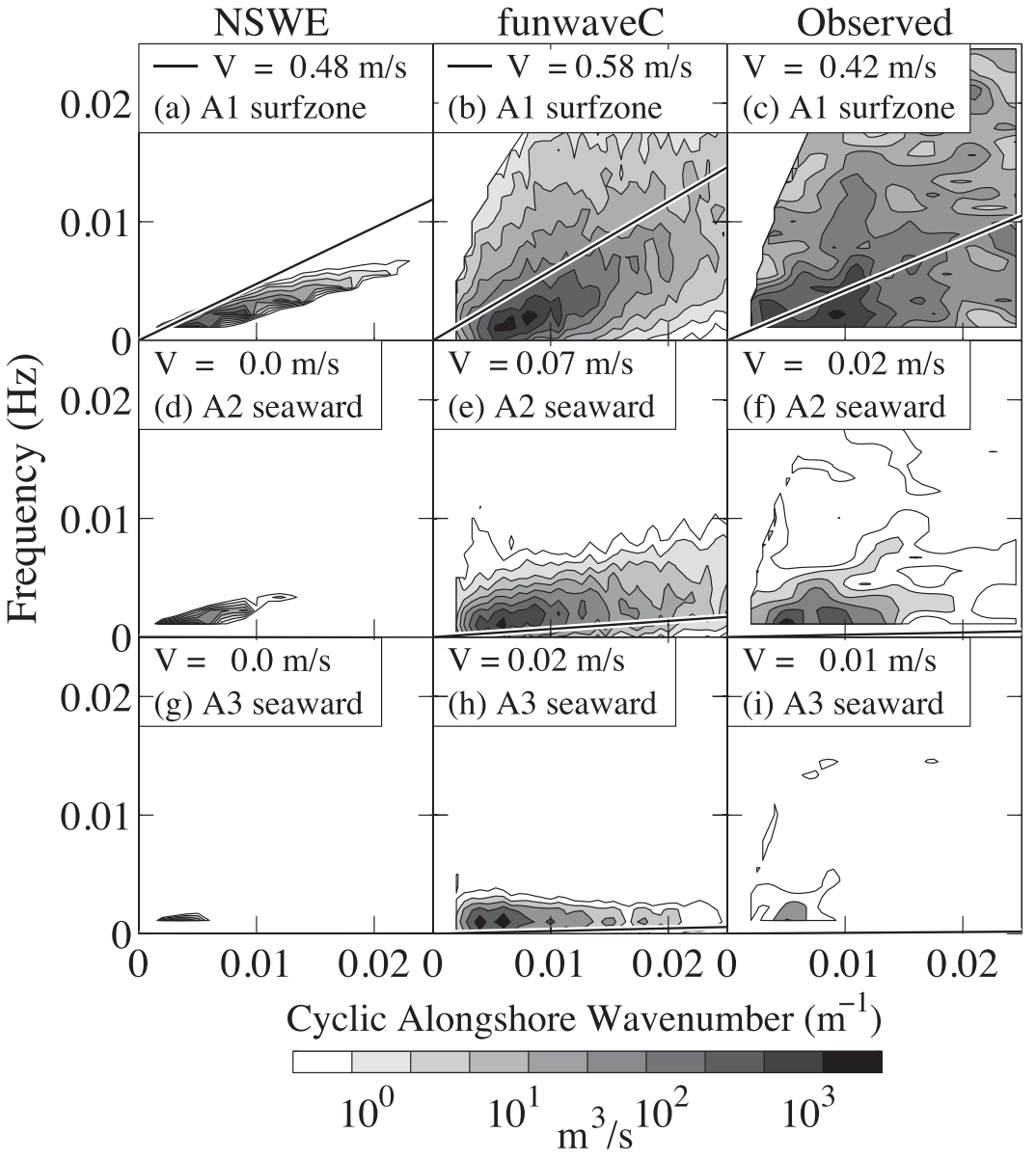

FIG. 3. SandyDuck experiment (0828) cross-shore velocity alongshore wavenumber frequency spectra $E(f, k_y)$ for (left) NSWE modeled, (center) funwaveC modeled, and (right) observed at cross-shore locations (top) A1 surfzone, (middle) A2 just seaward of the surfzone, and (bottom) A3 well seaward of the surfzone. The gravity wave region bounded by the mode zero edge wave dispersion is blanked out to the left of each panel. The local-mean alongshore current V (solid line) is given in the legend. The format of the figures is based on Noyes et al. (2005). The contour spacing is every $10^{2/5}$.

group breaking wave mechanisms. In addition, the steady-forcing NSWE model results of Noyes et al. are also presented to highlight the difference between a model that generates eddies only by a shear instability and the wave-resolving model that includes all mechanisms. As previously done (Noyes et al. 2005; Long and Özkan-Haller 2009), the $E(f, k_y)$ are only presented and compared in the downstream direction (i.e., with the alongshore current) as the rotation energy propagation is far larger in the downstream than upstream direction (Noyes et al. 2004).

On 0828 at the surfzone A1 location, the funwaveC $E(f, k_y)$ is qualitatively more similar to the observations than the NSWE (Figs. 3a–c). The NSWE $E(f, k_y)$ is a narrow ridge with energy concentrated at lower k_y ($<0.01\,\mathrm{m}^{-1}$) and f ($<0.004\,\mathrm{Hz}$), in contrast to the broader f and k_y range of $E(f, k_y)$ (up to $k_y = 0.024\,\mathrm{m}^{-1}$ and $f = 0.02\,\mathrm{Hz}$) in the funwaveC and observed. At a

specific k_y, the funwaveC and observed $E(f, k_y)$ ridge is wider in frequency than the NSWE $E(f, k_y)$. At A2 (Fig. 3, middle row), located just seaward of the surfzone, NSWE energy is reduced significantly to very low k_y, whereas the funwaveC and observed $E(f, k_y)$ are more qualitatively consistent. At A3 (bottom row of Fig. 3), the energy is weak everywhere. As discussed by Noyes et al. (2005), the $E(f, k_y)$ ridge slope generally is consistent with the local V (solid line in Fig. 3) at the three cross-shore locations, in contrast to equilibrated weakly nonlinear shear wave theory (Feddersen 1998). These results are qualitatively consistent with the wave group model results of Long and Özkan-Haller (2009), who showed that for an unstable alongshore current, the $E(f, k_y)$ extended to larger k_y when groups were present relative to no groups.

The features in the NSWE, funwaveC, and observed qualitative $E(f, k_y)$ comparison are similar on other days. On 1101 within the surfzone at A1 and A2, the observed $E(f, k_y)$ has a broad ridge with slope similar to the local V that extends to large $k_y = 0.024\,\mathrm{m}^{-1}$ and higher $f = 0.02$ Hz (Figs. 4c,f). The funwaveC modeled surfzone $E(f, k_y)$ have similar features as the observed (Figs. 4c,f). In contrast, the NSWE $E(f, k_y)$ have narrow ridges limited to $k_y \leq 0.01\,\mathrm{m}^{-1}$ (Figs. 4a,d). Seaward of the surfzone at A3 and A4, the observed and funwaveC $E(f, k_y)$ is limited to lower frequencies (largely $f < 0.005$ Hz) but a broad range of k_y (Figs. 4h,i,k,l). The A3 and A4 NSWE $E(f, k_y)$ is also confined to lower frequencies, but not a broad range of k_y (Figs. 4g,j).

These surfzone features (Figs. 3 and 4) also are clearly seen in the very wide (spanning A1–A5) surfzone of 1113 (Fig. 5). The observed $E(f, k_y)$ has a broad ridge that extends to large $k_y = 0.024\,\mathrm{m}^{-1}$ and higher $f = 0.025$ Hz (Fig. 5, right column). The funwaveC $E(f, k_y)$ are consistent with the observed (Fig. 5, middle column), whereas the NSWE $E(f, k_y)$ are again narrow ridges with reduced energy at larger k_y and f (Fig. 5, left column). Both model and observed $E(f, k_y)$ ridge slopes are consistent with the local V at all arrays.

On 1117, observed $E(f, k_y)$ could not be estimated at A1, located mid surfzone near the maximum V (Fig. 2k). Thus, the comparison is performed only at A2–A4 (Fig. 6). At the outer surfzone A2 (Fig. 2j), the observed and funwaveC $E(f, k_y)$ are similar and have general features consistent with the other case examples. At A2, the NSWE model $E(f, k_y)$ is most qualitatively similar to the observed of all the surfzone array cases. Although the ridge is not sufficiently broad, significant NSWE energy is present at higher k_y (up to $0.02\,\mathrm{m}^{-1}$, Fig. 6a) than all other case examples. Seaward of the surfzone at A3 and A4, the observed, funwaveC, and NSWE $E(f, k_y)$ have similar features to the other seaward of the surfzone locations in the other case examples.

c. Rotational velocities

At surfzone locations, the funwaveC modeled $E(f, k_y)$ is qualitatively far more consistent with the observed $E(f, k_y)$ than is the NSWE modeled $E(f, k_y)$ (Figs. 3–6). The comparison is now made quantitative by comparing the rotational velocities u_{rot} and v_{rot} associated with these $E(f, k_y)$ across all case example days within and seaward of the surfzone. Observed, NSWE modeled, and funwaveC modeled rms rotational (i.e., vortical) velocities u_{rot} and v_{rot} are calculated by integrating the respective $E(f, k_y)$ over the nongravity wave region between $f = 0.001\,65$ Hz and $f = 0.05$ Hz and over alongshore wavenumber k_y outside of the gravity wave region and taking a square root [see Noyes et al. (2004), for processing details]. This procedure removes irrotational infragravity wave energy, leaving only rotational (eddy) velocity contributions.

At surfzone locations, the observed u_{rot} varies between 0.08 and $0.21\,\mathrm{m\,s}^{-1}$ and v_{rot} between 0.07 and $0.16\,\mathrm{m\,s}^{-1}$ (black asterisks in Fig. 7). The funwaveC model rotational velocities are similar to the surfzone observed u_{rot} and v_{rot} (Figs. 7a,b, respectively), with combined u_{rot} and v_{rot} rms errors of $0.045\,\mathrm{m\,s}^{-1}$ and small bias. The funwaveC model rotational velocity skill is 0.87. Skill (relative to zero prediction) is defined as (Feddersen et al. 2011)

$$\mathrm{skill} = 1 - \langle [u_{\mathrm{rot}}^{(\mathrm{obs})} - u_{\mathrm{rot}}^{(\mathrm{m})}]^2 + [v_{\mathrm{rot}}^{(\mathrm{obs})} - v_{\mathrm{rot}}^{(\mathrm{m})}]^2 \rangle / \langle [u_{\mathrm{rot}}^{(\mathrm{obs})}]^2 + [v_{\mathrm{rot}}^{(\mathrm{obs})}]^2 \rangle,$$

where superscripts (m) and (obs) denote model and observed quantities, respectively, and angle brackets denote an average over all surfzone observations. The NSWE model generally underpredicts the observed surfzone u_{rot} and v_{rot} significantly (Figs. 7c,d) with larger combined rms errors $0.085\,\mathrm{m\,s}^{-1}$, large bias, and skill of 0.55. Seaward of the surfzone locations (circles in Fig. 7), u_{rot} and v_{rot} are $\leq 0.04\,\mathrm{m\,s}^{-1}$, much weaker than within the surfzone. The funwaveC and NSWE model rotational velocities are similar to the observed seaward of the surfzone u_{rot} and v_{rot}. Note that the combined u and v seaward of the surfzone rms errors are larger for funwaveC ($0.02\,\mathrm{m\,s}^{-1}$) than for the NSWE model ($0.01\,\mathrm{m\,s}^{-1}$).

5. Results: Vorticity

The ability of the funwaveC model to reproduce the observed surfzone eddy field (section 4) means that funwaveC can be used to diagnose the dominant processes generating surfzone eddies. The model sea surface elevation η and perturbation vorticity ω' snapshots for 0828 are shown in Fig. 8 as an example of the

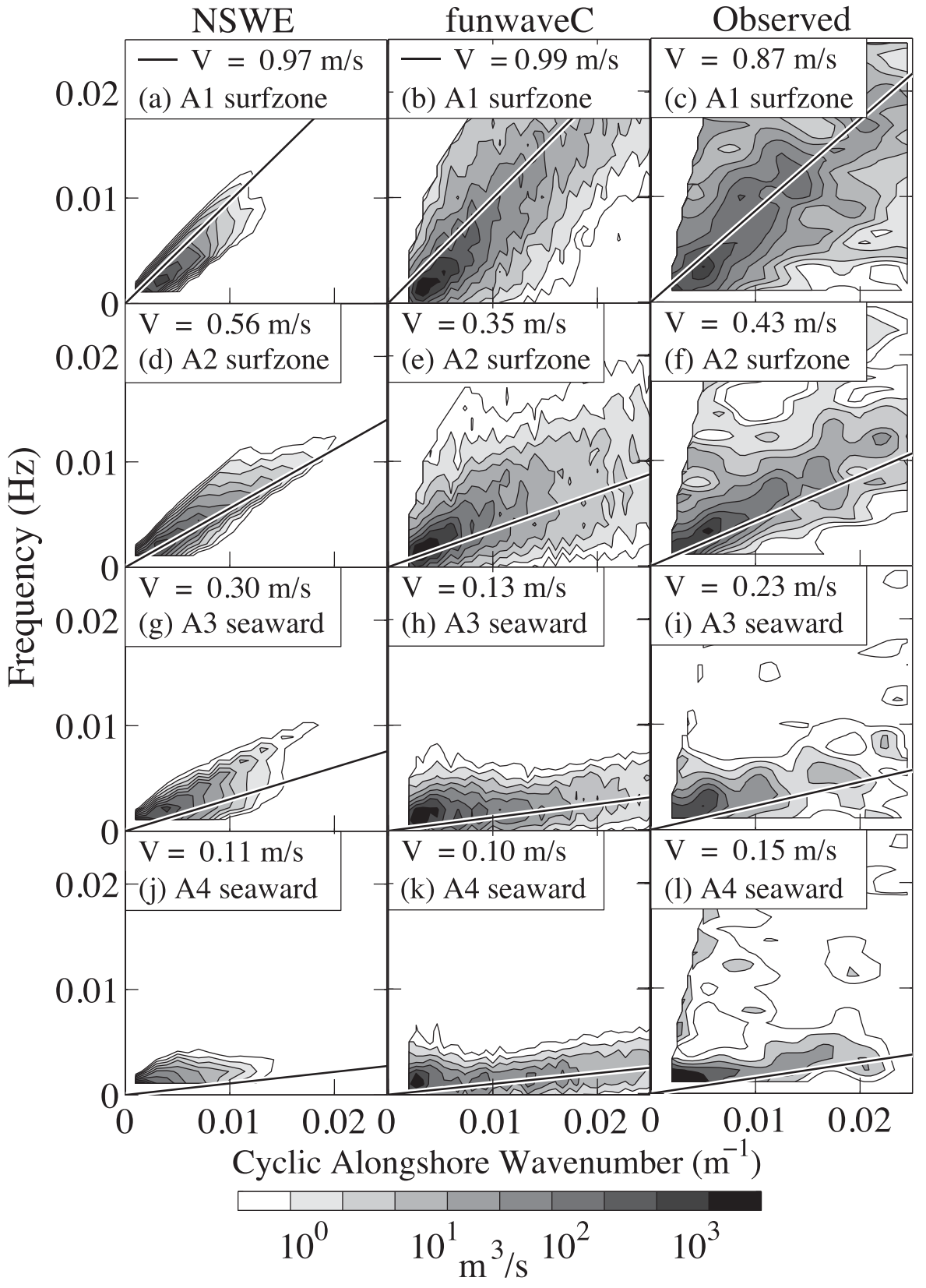

FIG. 4. SandyDuck experiment (1101) cross-shore velocity alongshore wavenumber frequency spectra $E(f, k_y)$ for (left) NSWE modeled, (middle) funwaveC modeled, and (right) observed at cross-shore locations (from top to bottom) A1–A4. See Fig. 3 for further details.

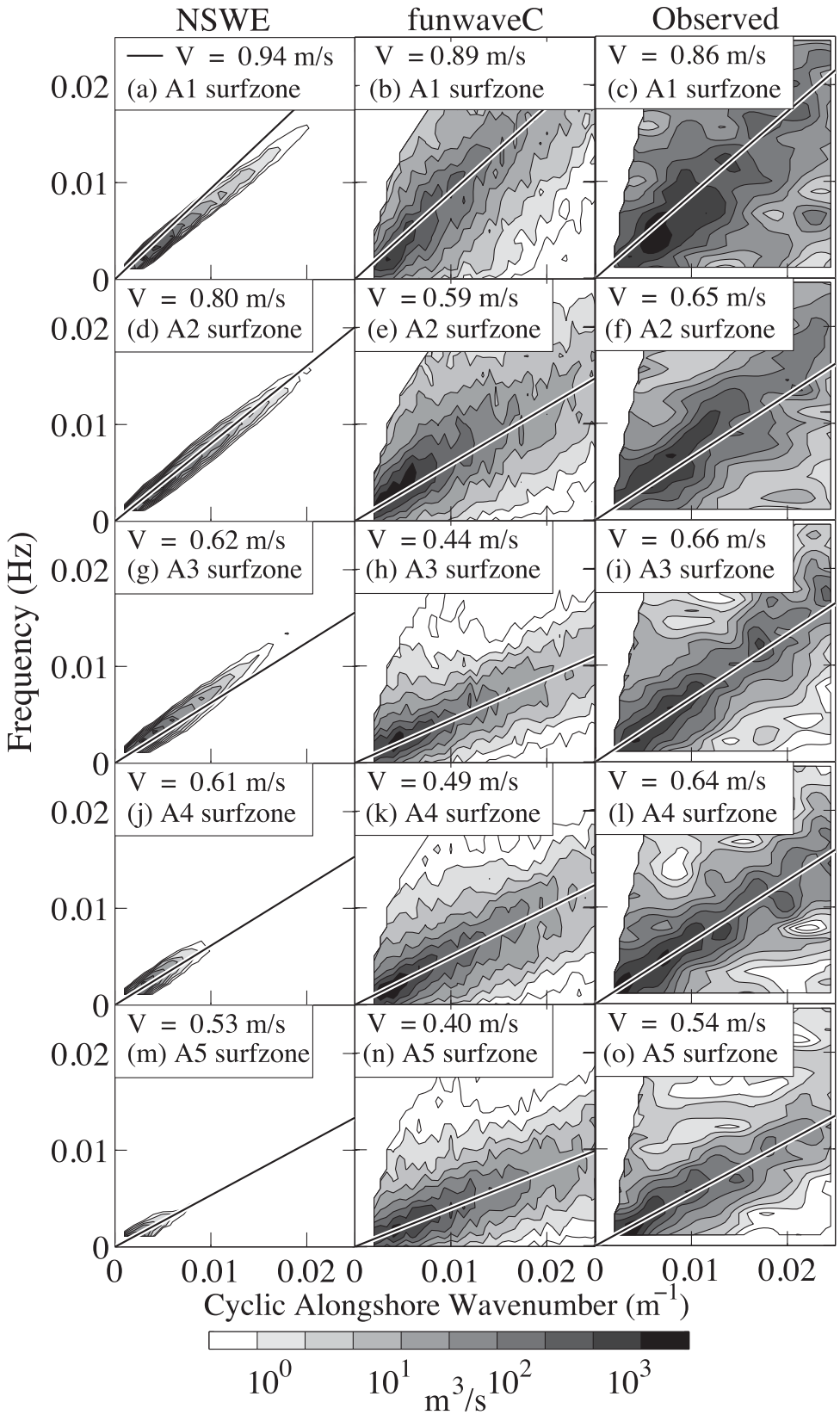

FIG. 5. SandyDuck experiment (1113) cross-shore velocity alongshore wavenumber–frequency spectra $E(f, k_y)$ for (left) NSWE modeled, (middle) funwaveC modeled, and (right) observed at cross-shore locations (from top to bottom) A1–A5 that are all within the surfzone. See Fig. 3 for further details.

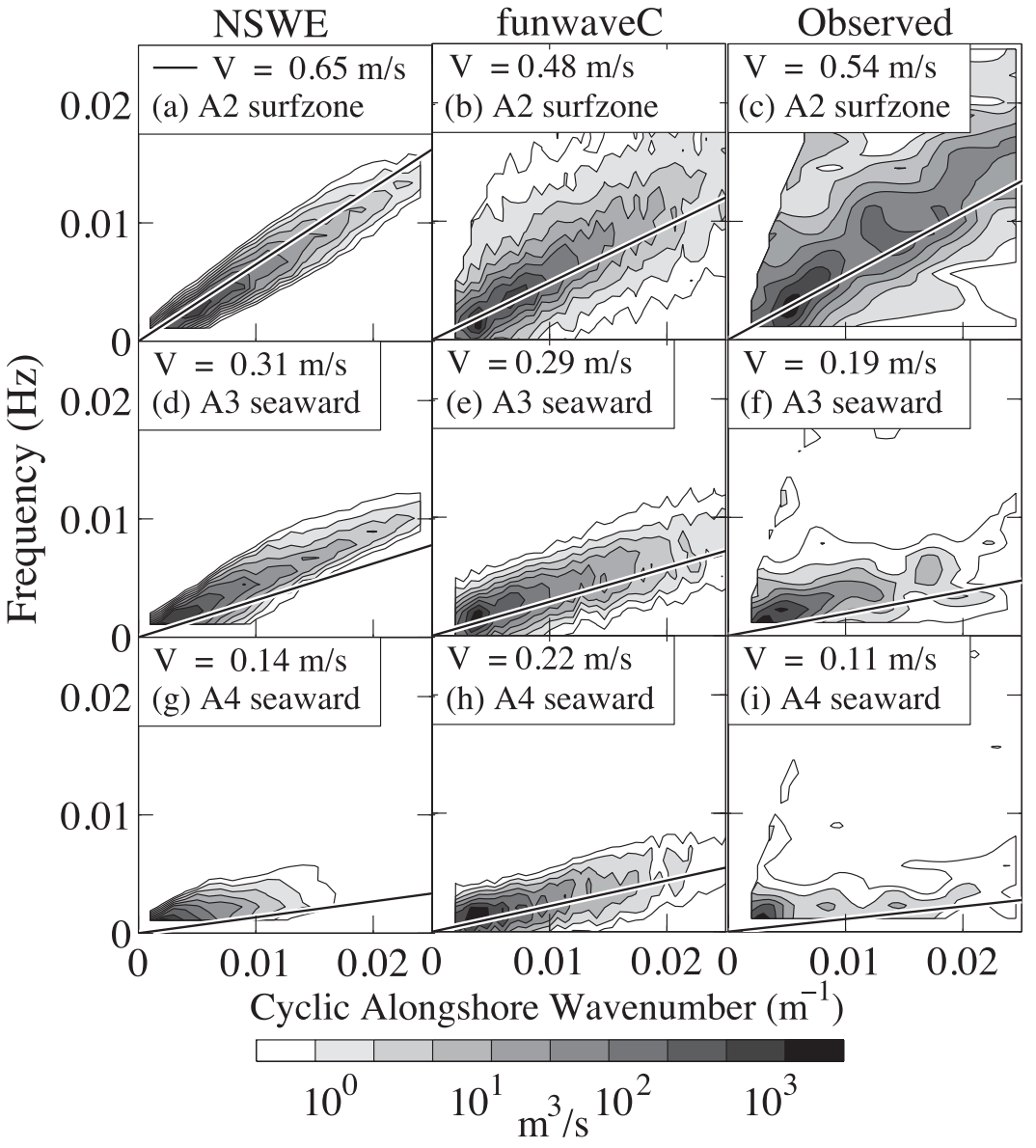

FIG. 6. SandyDuck experiment (1117) cross-shore velocity alongshore wavenumber–frequency spectra $E(f, k_y)$ for (left) NSWE modeled, (middle) funwaveC modeled, and (right) observed at cross-shore locations (top) A2, (middle) A3, and (bottom) A4. See Fig. 3 for further details.

modeled surfzone eddy field. The perturbation vorticity ω' is defined as the difference from the time- and alongshore-averaged mean vorticity. A broadbanded, obliquely incident, and directionally spread wave field approaches the beach with wave breaking beginning at approximately $x_b = 190$ m (Fig. 8a). Within the surfzone (dashed line in Fig. 8a), perturbation vorticity ω' is present at a broad range of length scales between 20 and 100 m. (Fig. 8b). Occasionally, eddies (patches of ω') are ejected seaward from the surfzone [see $(x, y) = (230, 20)$ m in Fig. 8b]. Note that for the case examples, the frequency spectra of surfzone vorticity (and potential vorticity) are red with most variance occurring well below the incident wave frequency range. The dominant forcing mechanisms for these eddies are examined next. Vorticity ω and perturbation vorticity ω' are the natural variables to diagnose competing surfzone eddy generation mechanisms as they correspond only to the (rotational) eddies and not the (irrotational) sea swell and infragravity band wave motions. Note, however, that examination of vorticity over velocity emphasizes shorter length scales.

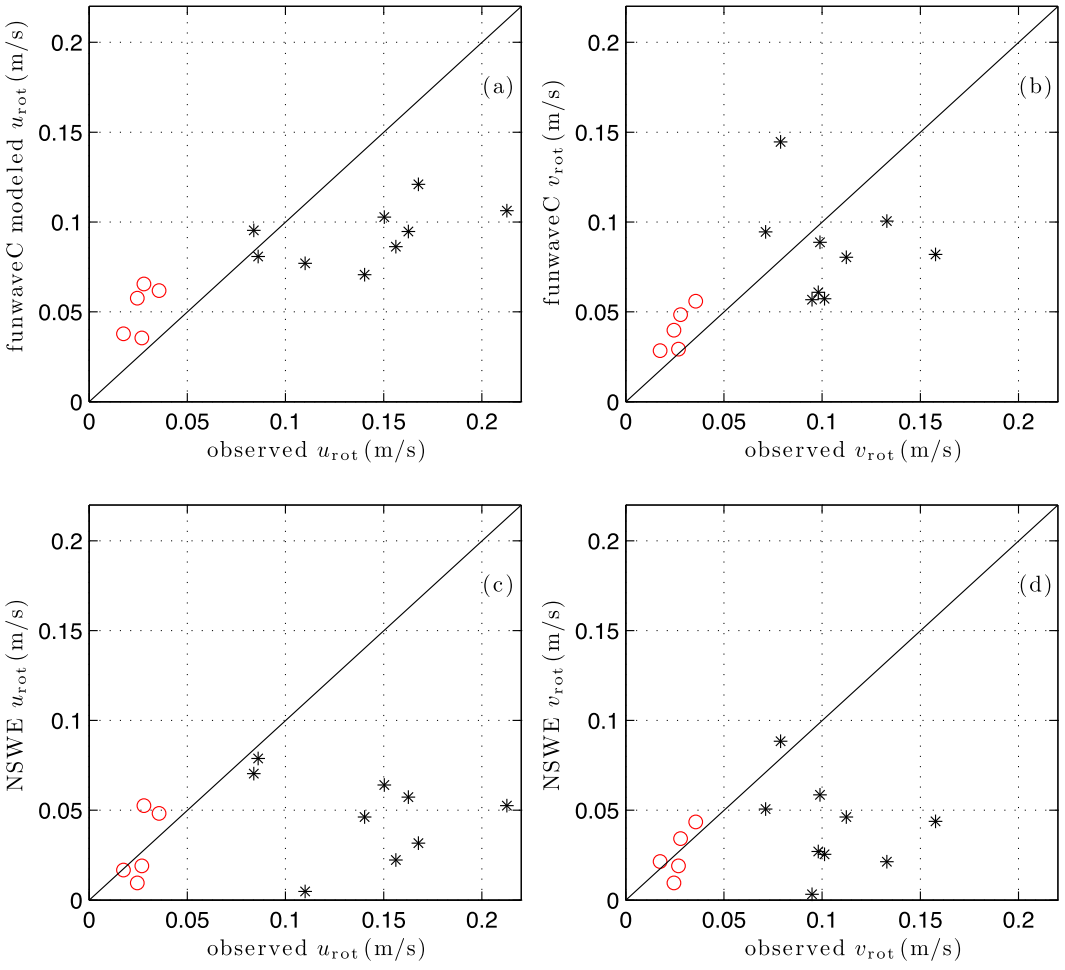

FIG. 7. Modeled vs observed rotational velocities (left) $u_{\rm rot}$ and (right) $v_{\rm rot}$ for (a),(b) funwaveC and (c),(d) NSWE at locations within (black asterisks) and seaward (red circles) of the surfzone. The black line represents the 1:1 relationship.

a. Mean squared perturbation vorticity budget

To diagnose the relative importance of shear instabilities or breaking wave vorticity forcing to the surfzone eddy field, the mean square perturbation vorticity $\overline{\omega'^2}$ (where the overbar represents an average) is examined. Beginning with the shallow-water-based vorticity equation, removing the mean, multiplying by ω', and averaging yields the $\overline{\omega'^2}$ evolution equation (e.g., Salmon 1998):

$$\frac{1}{2}\frac{\partial\overline{\omega'^2}}{\partial t}+\cdots=-\overline{\omega' u'}\frac{d^2V}{dx^2}+\overline{\omega'\nabla\times\mathbf{F}_{\rm br}}+\cdots, \quad (3)$$

where the first and second terms on the rhs of (3) are the shear instability and breaking wave contributions, respectively. Other terms not shown in (3) are the advection and vortex stretching terms that transform but do not generate eddies and the bottom-friction-induced $\overline{\omega'^2}$ decay. The equation for $\overline{\omega'^2}$ is considered here for simplicity, but the equation for mean square perturbation potential vorticity, considered by Long and Özkan-Haller (2009) who integrated across the surfzone, yields identical results, as does examining the magnitude of terms in the perturbation vorticity equation. The first and second terms on the rhs of (3) are estimated from the 1-Hz model output with the overbar representing both a time average (over last 5000 s of model run) and an alongshore average over the domain, implying that $\overline{\phi(x,y,t)}=\bar{\phi}(x)$. Thus, both rotational and irrotational motions contribute to $\overline{u'\omega'}$. The results are nearly identical if the perturbation rotational velocity u' (which only has a low-frequency component), derived from a rotational–irrotational velocity decomposition (Spydell and Feddersen 2009), is used instead of the full u'.

The breaking wave vorticity forcing ($\overline{\omega'\nabla\times\mathbf{F}_{\rm br}}$) dominates over the shear instability mechanism ($\overline{\omega' u'}d^2V/dx^2$) at all cross-shore locations and for all case

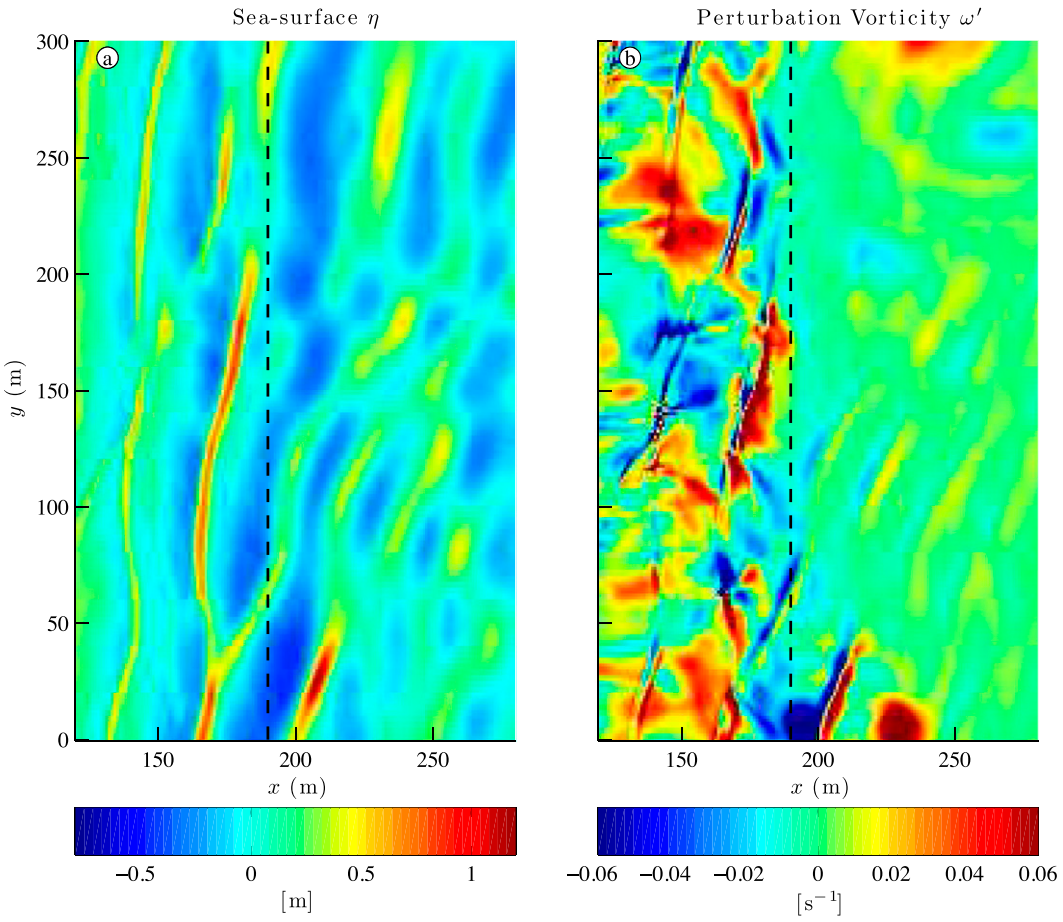

FIG. 8. Horizontal x, y snapshot of modeled (a) sea surface elevation η and (b) perturbation vorticity ω' for 0828 at $t = 5000$ s into the model simulation. The shoreline is at approximately $x = 110$ m, and the black dashed line ($x_b = 190$ m) is the approximate outer limit of the surfzone. Only a subset of the model domain is shown. Note the broad range of perturbation vorticity length scales within the surfzone.

examples (cf. blue- and green-dashed curves in Fig. 9). Within the surfzone, the breaking wave term has a magnitude from 10^{-5} to 6×10^{-5} s^{-3} across all days. On all days, the shear instability term is negligible compared to the breaking wave term (Fig. 9). On 0828, 1101, and 1117, the breaking wave term is 100 times larger in magnitude than the shear production term when averaged across the surfzone. On 1113, the breaking wave term is three orders of magnitude larger. Although the mean alongshore current shear dV/dx can be quite large (up to 0.01 s^{-1}), surfzone eddies in these four case examples were generated by the curl of breaking wave forcing and not by shear instability.

b. *Alongshore length scales of vorticity forcing and vorticity*

Given that the shear instability mechanism is negligible relative to the breaking wave vorticity forcing in driving surfzone eddies, the remaining question is: what is the relative importance of wave group forcing (with long alongshore length scales) or individual breaking waves (with shorter length scales) in driving surfzone eddies? This question is addressed by examining the cross-surfzone-averaged (indicated with a hat) alongshore wavenumber spectra of the breaking wave vorticity forcing $\hat{E}_{\mathbf{V}\times\mathbf{F}_{\mathrm{br}}}(k_y)$ and the vorticity $\hat{E}_{\omega}(k_y)$. Owing to the cross-shore averaging and to account for vortex stretching effects, potential vorticity $\xi = \omega/d$ and breaking wave potential vorticity forcing $d^{-1}\mathbf{V} \times \mathbf{F}_{\mathrm{br}}$, where $d = \eta + h$, are calculated from the model output. At a particular cross-shore location, the alongshore wavenumber spectra of potential vorticity $E_{\xi}(x, k_y)$ and breaking wave potential vorticity forcing $E_{d^{-1}\nabla\times\mathbf{F}_{\mathrm{br}}}(x, k_y)$ are estimated by time-averaging 1-Hz alongshore periodograms over the 5000 s of model output at various cross-shore surfzone locations. These spectra are then cross-shore averaged from the shoreline to the "breakpoint" to arrive at a single surfzone-averaged spectra,

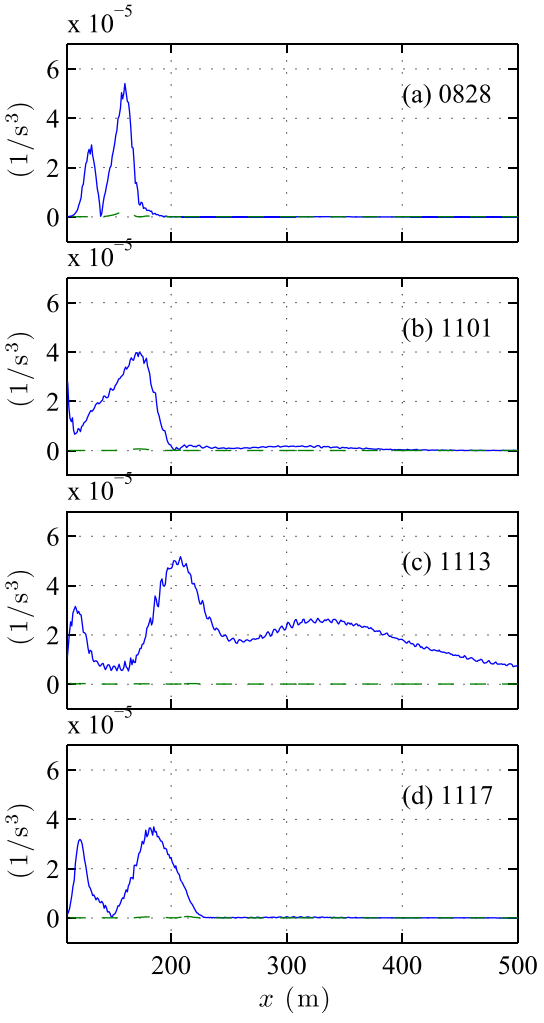

FIG. 9. The breaking wave forcing $|\overline{\omega' \mathbf{V} \times \mathbf{F}_{\mathrm{br}}}|$ (blue) and shear instability $|\overline{\omega' u'} d^2 V/dx^2|$ (green dashed) term magnitude in the mean perturbation vorticity squared budget (3) vs FRF cross-shore coordinate x for the four case examples: (a) 0828, (b) 1101, (c) 1113, and (d) 1117.

indicated with a caret, that is, $\hat{E}_{\xi}(k_y)$. The cross-surfzone-averaged potential vorticity spectrum is converted to a vorticity spectrum by multiplying by the mean surfzone water depth squared $\bar{d}^2$, for example,

$$\hat{E}_{\omega}(k_y) = \hat{E}_{\xi}(x, k_y)\bar{d}^2. \tag{4}$$

Similarly the cross-surfzone-averaged breaking wave potential vorticity forcing is converted to the forcing spectrum $\hat{E}_{\nabla \times \mathbf{F}_{\mathrm{br}}}(k_y)$ by multiplying by $\bar{d}^2$. The results do not change if the cross-shore-averaged vorticity or potential vorticity is used.

In all case examples, $\hat{E}_{\nabla \times \mathbf{F}_{\mathrm{br}}}(k_y)$ is broad in k_y (Fig. 10, left column). On 0828, 1101, and 1113, $\hat{E}_{\nabla \times \mathbf{F}_{\mathrm{br}}}(k_y)$ is white (flat) for $k_y < 0.02\,\mathrm{m}$, has a maximum roughly twice the background value between $0.05 < k_y < 0.12\,\mathrm{m}^{-1}$ [denoted by vertical arrows in Figs. 10a(1), 10b(1), and 10d(1)], and decays at higher k_y. On 1113 with a wide surfzone, $\hat{E}_{\nabla \times \mathbf{F}_{\mathrm{br}}}(k_y)$ is essentially white at all k_y. For all case examples, between 80% (0828 and 1101) and 90% (1117) of the $\nabla \times \mathbf{F}_{\mathrm{br}}$ variance is at $k_y > 0.05\,\mathrm{m}^{-1}$, equivalent to alongshore length scales <20 m. The vorticity forcing magnitude varies significantly cross surfzone, but the spectral shape does not (red dashed lines in Fig. 10, left). Therefore, the forcing length scales do not vary significantly across the surfzone.

The surfzone-averaged vorticity spectrum $\hat{E}_{\omega}(k_y)$ that results from the vorticity forcing is generally red at $k_y > 10^{-2}\,\mathrm{m}^{-1}$ with a steep falloff at $k_y > 10^{-1}\,\mathrm{m}^{-1}$ (Fig. 10, right). Although vorticity forcing is concentrated at $k_y > 0.05\,\mathrm{m}^{-1}$ (<20 m length scale), longer length scales contribute to vorticity variance. Between 75% (1113) and 40% (0828) of the vorticity variance is at $k_y > 0.01\,\mathrm{m\,s}^{-1}$ (<100 m scales). The red vorticity spectrum can indicate 2D turbulence with nonlinear energy transfers from the higher k_y (>$0.05\,\mathrm{m}^{-1}$) vorticity forcing to lower k_y (e.g., Tabeling 2002) or may indicate an amplified vorticity response to forcing at smaller k_y (e.g., MacMahan et al. 2010).

The detailed structure of $\hat{E}_{\omega}(k_y)$ varies across case example days with no consistent $\hat{E}_{\omega}(k_y) \propto k_y^{\gamma}$ power-law structure (indicated with dashed–dotted lines in Fig. 10, right). The $\hat{E}_{\omega}(k_y)$ power-law exponent γ has a shift near the maximum in the vorticity forcing for the three case examples (0828, 1101, and 1117) with a clear vorticity forcing maximum (Figs. 10,a,b,d). In classic 2D turbulence forced at a single k_F (e.g., Kraichnan and Montgomery 1980), the velocity spectrum $E_v(k_y)$ has power-law exponent $-5/3$ at $k < k_F$ (energy cascade regime) and power-law exponent -3 at $k > k_F$ (enstrophy cascade regime). In an isotropic flow, vorticity and velocity wavenumber spectrum are related by $\hat{E}_{\omega}(k_y) \propto k_y^2 \hat{E}_v(k_y)$, the $-5/3$ energy cascade power-law exponent corresponds to $\gamma = 1/3$, and the -3 enstrophy cascade exponent corresponds to $\gamma = -1$. Although the surfzone-averaged $\hat{E}_{\omega}(k_y)$ exhibit characteristics of 2D turbulence, classic energy $\gamma = 1/3$ or enstrophy $\gamma = -1$ cascade regimes are not regularly exhibited (Fig. 10, right). This is discussed in section 6.

6. Discussion

A model must accurately simulate both magnitude and length scales of the surfzone eddies to properly represent surfzone tracer mixing. The qualitative similarity across all k_y between funwaveC and observed $E(f, k_y)$ (Figs. 3–6) and the quantitative similarity between u_{rot} and v_{rot} (Fig. 7) indicates that the funwaveC model is

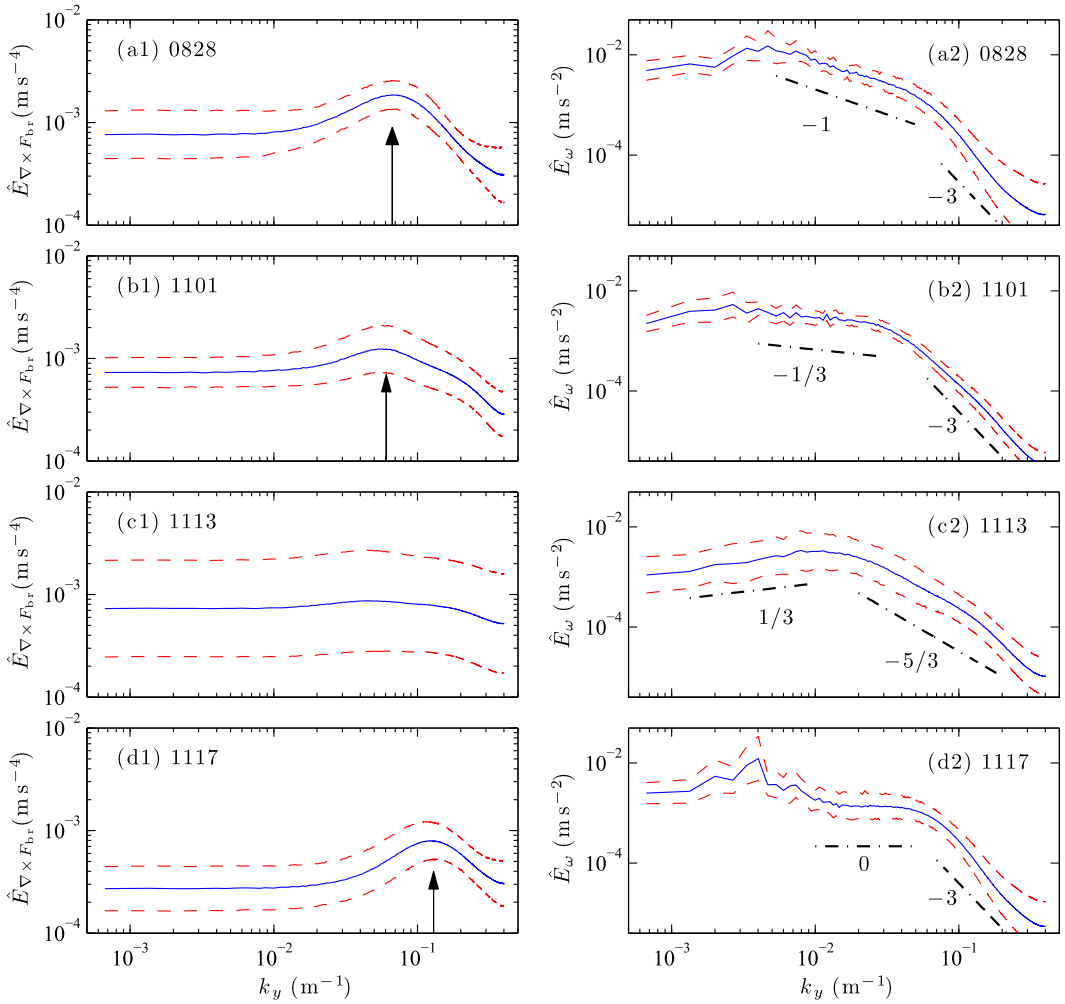

FIG. 10. The cross-surfzone mean (solid blue) and ± standard deviation (red dashed) of (left) breaking wave vorticity forcing $\hat{E}_{\mathbf{V}\times\mathbf{F}_{\rm br}}$ and (right) vorticity $\hat{E}_{\omega}$ spectra (4) vs alongshore wavenumber k_y for (a) 0828, (b) 1101, (c) 1113, and (d) 1117. In the left column, the vertical arrows in (a1),(b1), and (d1) indicate the wavenumber when a distinct maximum $\hat{E}_{\mathbf{V}\times\mathbf{F}_{\rm br}}$ occurs. On 1113, there was no distinct maximum. In the right column, the dashed–dotted lines indicate approximate power law regions in which $E_{\omega} \propto k_y^{\gamma}$, where the γ value is indicated near the dashed line. The Nyquist wavenumber is $k_y = 0.4\,\mathrm{m}^{-1}$.

accurately simulating the surfzone eddy field during these four SandyDuck case examples. This is consistent with the funwaveC model–data comparison from the HB06 experiment (Feddersen et al. 2011),which compared $u_{\rm rot}$ and $v_{\rm rot}$ derived from a different estimator (Lippmann et al. 1999), as $E(f, k_y)$ could not be estimated. It is also consistent with the funwaveC reproducing the HB06 experiment observed tracer-derived surfzone diffusivity (Clark et al. 2011).

With a WR model, the extrinsic breaking wave vorticity forcing was found to completely dominate over the intrinsic shear instability mechanism through an analysis of the mean squared perturbation vorticity (Fig. 9). In contrast, with a group-forced WA model for an idealized moderate V surfzone example, Long and Özkan-Haller (2009) found that breaking wave vorticity forcing and shear instability contributed approximately equally through a similar analysis. This difference likely is due to the WA model not including the forcing at short scales (particularly <20 m) that dominates the forcing variance (Fig. 10, left). However, for all four cases here, the incident wave field was broader in frequency (2 times) and in wave directional spread than the case considered by Long and Özkan-Haller, which would enhance the breaking wave vorticity forcing relative to shear instability. However, these four cases also had large V and strong shear, which is linked to enhancing shear instability (e.g., Dodd and Thornton 1990). Given the

dominance of the breaking wave vorticity forcing over these strong shear conditions, one may conclude that in most natural surfzones the shear instability eddy generation mechanism is negligible relative to the breaking wave forcing in the vorticity dynamics, with possible exceptions for very narrowbanded, highly oblique large incident waves.

Wave breaking forces vorticity predominantly at <20 m scales (Fig. 10, left). Some fraction of this vorticity forcing is dissipated through bottom friction, and some fraction must be transferred to longer scales (smaller k_y) through a nonlinear 2D turbulent eddy cascade that could create a broad vorticity sprectrum. Vorticity forcing at these relatively short scales is consistent with the presence of surfzone eddies with length scales 10–50 m inferred from the two-particle diffusivity estimated with observed and modeled surfzone drifters when $V = 0\,\mathrm{m\,s^{-1}}$ (Spydell et al. 2007; Spydell and Feddersen 2009). It is also consistent with eddy energy present out to $k_y = 0.05\,\mathrm{m^{-1}}$ in WR transient rip current modeling (Johnson and Pattiaratchi 2006). This interpretation contrasts with a wave-averaged VLF surfzone eddy model directly forced by wave groups when $V \approx 0\,\mathrm{m\,s^{-1}}$ (MacMahan et al. 2010). This linear wave group model, which neglects nonlinear energy transfers, generates rms surfzone eddy velocities correlated with, but 40% larger than, observed (MacMahan et al. 2010). However, except for a single case example, eddy length scales were not generally examined.

Wave group models generally require that the incident wave spectrum be narrow in frequency and direction (e.g., Van Dongeren et al. 2003; Reniers et al. 2004). This implies that, for near-normally incident mean wave angles, $\Delta k_y/|\overline{\mathbf{k}}| \ll 1$, where $|\overline{\mathbf{k}}|$ and Δk_y are the mean wavenumber magnitude and spread of the incident wave alongshore wavenumber spectrum. For the incident wave parameters (Table 1), the mean wavelength $2\pi|\overline{\mathbf{k}}|^{-1}$ ranges between 50 and 70 m. This implies that the alongshore group scale must be much greater than this wavelength for a wave group model to accurately represent the groups. However, for these cases, the directional spread (Table 1) is so large that the narrowbanded requirements of the model are violated.

Given the short length scales ($k_y > 0.05\,\mathrm{m^{-1}}$) of the WR breaking wave vorticity forcing, this suggests that a WA model with group forcing may not accurately simulate eddy length scales smaller than the surfzone width (here ~100 m) that are important to surfzone mixing (e.g., Spydell et al. 2007; Clark et al. 2010, 2012). The vorticity spectrum is often red, and the vorticity source at longer scales is uncertain, which may be due to a 2D turbulence inverse energy cascade bringing energy to smaller k_y or may result from an amplified vorticity response to direct forcing at smaller k_y (MacMahan et al. 2010).

As 2D turbulence is not a ''wave'' with a distinct dispersion relationship, it is naturally studied in wavenumber space (e.g., Kraichnan and Montgomery 1980). Both Noyes et al. (2005) and Long and Özkan-Haller (2009) discussed that alongshore eddy advection yields a $E(f, k_y)$ ridge slope approximately equal to the local V. More specifically, for an assumed ''frozen'' turbulence field, alongshore eddy advection induces a ''Taylor hypothesis'' mapping from wavenumber to frequency via $f = k_y V$, giving the appearance of a shear wave dispersion relationship (e.g., Oltman-Shay et al. 1989; Noyes et al. 2004). This explains why VLF ($f < 0.004$ Hz) energy is observed to be prevalent during weak V conditions (MacMahan et al. 2010). With this interpretation, VLF energy is not dynamically distinct from infragravity band (IG: $0.004 < f < 0.03$ Hz) rotational energy. With the same eddy field, but stronger V, eddy k_y variability would be mapped to a higher frequency than the observed VLF. The observed and funwaveC modeled $E(f, k_y)$ ridge frequency broadening at higher k_y (see A1 on 0828, Fig. 3) possibly could be explained by oscillating advection of larger k_y motions by smaller k_y motions resulting in increasing frequency spreading (e.g., Lumley and Terray 1983).

The near-white $\hat{E}_{\mathbf{V}\times\mathbf{F}_{\mathrm{br}}}(k_y)$ spectrum with a high k_y ($>0.1\,\mathrm{m^{-1}}$) falloff (Fig. 10, left) is approximately consistent with surfzone stochastic vorticity forcing with an $O(10)$-m length scale. This also is consistent breaking-wave-induced vorticity changes observed at similar length scales (Clark et al. 2012). This suggests that the effect of short-crested breaking wave vorticity generation could be stochastically parameterized within a wave-averaged model, analogous to the stochastic breaking wave forcing of the mixed layer by Sullivan et al. (2007). However, the appropriate statistical distribution of this stochastic forcing and how it depends on the incident wave field is not understood.

There are many reasons to expect that the surfzone $\hat{E}_{\omega}(k_y)$ does not consistently exhibit 2D turbulence classic energy or enstrophy cascade regimes (Fig. 10, right). Classic 2D turbulence (e.g., Kraichnan and Montgomery 1980; Boffetta and Ecke 2012) assumes isotropy and forcing at a single wavenumber k_F that is broadly separated between the domain scale and the scale of enstrophy dissipation. In contrast, the stochastic vorticity forcing here is broad in wavenumber k_y space and may not be isotropic. In addition, the surfzone is not isotropic owing to the shoreline boundary and the cross-shore varying depth. Furthermore, the ~100-m-wide (except 1113) surfzone region within which eddies are forced imposes an additional length scale. Last, the sheared

alongshore current may also deform eddies away from isotropy. These factors all potentially lead to differences from classic 2D turbulence, and result in a complex and interesting eddy field. Future work will examine the structure of the surfzone eddy field and how eddies transform as they leave the surfzone where the depth increases and the forcing ceases.

7. Summary

Here, the wave-resolving (WR) Boussinesq model funwaveC is used to simulate four case examples from the SandyDuck field experiment presented by Noyes et al. (2005). The model funwaveC is initialized with the observed bathymetry and incident wave energy, mean direction, and directional spread at each frequency. For these four cases, the funwaveC model largely reproduces the predicted cross-shore significant wave height H_s and mean alongshore current V (section 4a). The funwaveC modeled $E(f, k_y)$ spectra (section 4b) and bulk rotational velocities (section 4c) are consistent with the observations. This gives confidence that the model can be used to diagnose eddy dynamics. Using the mean squared perturbation vorticity budget (section 5a), breaking wave vorticity forcing dominates the shear instability mechanism, showing that in these cases the surfzone eddies are not generated by a shear instability mechanism. As these cases have strong V and large mean velocity shear, this likely applies to most surfzones with possible exceptions for very narrow banded—in frequency and direction—highly oblique, incident waves.

The alongshore wavenumber spectra of breaking wave vorticity forcing is broad with the majority (>80%) of vorticity forcing occurring at short alongshore scales (<20 m). Only a wave-resolving model can force vorticity at these scales. However, the alongshore wavenumber spectra of vorticity is red. This may result from a 2D turbulence inverse energy cascade bringing energy from short to long length scales. Yet, the vorticity spectra did not follow classic 2D turbulence power-law scalings, possibly due to the broad forcing, the finite cross-shore forcing region, and cross-shore variable depth. Alternatively, the red vorticity alongshore wavenumber spectrum also may result from an amplified vorticity response to direct forcing at smaller k_y.

Acknowledgments. This work was funded by the National Science Foundation and the Office of Naval Research. ONR funded the SandyDuck field experiment. S. Elgar, T. H. C. Herbers, R. T. Guza, and B. Raubenheimer were PIs on the PUV array component of the experiment used here. The instruments were deployed and maintained by staff from the Center for Coastal Studies, Scripps Institution of Oceanography. Staff from the U.S. Army Corps of Engineers Field Research Facility, Duck, North Carolina, provided processed survey data and data from their pressure array in 8-m water depth. (The open-source funwaveC model developed by F. Feddersen is available at http://falk.ucsd.edu.) Matthew Spydell provided useful feedback on the manuscript. The author would also like to thank two anonymous reviewers whose critical examination helped improve the manuscript significantly.

REFERENCES

Allen, J. S., P. A. Newberger, and R. A. Holman, 1996: Nonlinear shear instabilities of alongshore currents on plane beaches. *J. Fluid Mech.,* **310,** 181–213.

Boffetta, G., and R. E. Ecke, 2012: Two-dimensional turbulence. *Annu. Rev. Fluid Mech.,* **44,** 427–451, doi:10.1146/annurev-fluid-120710-101240.

Bowen, A. J., and R. A. Holman, 1989: Shear instabilities of the mean longshore current: 1. Theory. *J. Geophys. Res.,* **94** (C12), 18 023–18 030.

Brown, J., J. H. MacMahan, A. Reniers, and E. Thornton, 2009: Surf zone diffusivity on a rip-channeled beach. *J. Geophys. Res.,* **114,** C11015, doi:10.1029/2008JC005158.

Chen, Q., J. T. Kirby, R. A. Dalrymple, S. Fengyan, and E. B. Thornton, 2003: Boussinesq modeling of longshore currents. *J. Geophys. Res.,* **108,** 3362, doi:10.1029/2002JC001308.

Clark, D. B., F. Feddersen, and R. T. Guza, 2010: Cross-shore surfzone tracer dispersion in an alongshore current. *J. Geophys. Res.,* **115,** C10035, doi:10.1029/2009JC005683.

——, ——, and ——, 2011: Modeling surfzone tracer plumes: 2. Transport and dispersion. *J. Geophys. Res.,* **116,** C11028, doi:10.1029/2011JC007211.

——, S. Elgar, and B. Raubenheimer, 2012: Vorticity generation by short-crested wave breaking. *Geophys. Res. Lett.,* **39,** L24604, doi:10.1028/2012GL054034.

Dodd, N., and E. Thornton, 1990: Growth and energetics of shear-waves in the nearshore. *J. Geophys. Res.,* **95** (C9), 16 075–16 083.

——, J. Oltman-Shay, and E. B. Thornton, 1992: Shear instabilities in the longshore current: A comparison of observation and theory. *J. Phys. Oceanogr.,* **22,** 62–82.

Elgar, S., R. T. Guza, W. C. O'Reilly, B. Raubenheimer, and T. H. C. Herbers, 2001: Wave energy and direction observed near a pier. *J. Waterw. Port Coastal Ocean Eng.,* **127,** 2–6.

Feddersen, F., 1998: Weakly nonlinear shear waves. *J. Fluid Mech.,* **372,** 71–91.

——, 2007: Breaking wave induced cross-shore tracer dispersion in the surfzone: Model results and scalings. *J. Geophys. Res.,* **112,** C09012, doi:10.1029/2006JC004006.

——, and R. T. Guza, 2003: Observations of nearshore circulation: Alongshore uniformity. *J. Geophys. Res.,* **108,** 3006, doi:10.1029/2001JC001293.

——, ——, S. Elgar, and T. H. C. Herbers, 1998: Alongshore momentum balances in the nearshore. *J. Geophys. Res.,* **103** (C8), 15 667–15 676.

——, D. B. Clark, and R. T. Guza, 2011: Modeling of surfzone tracer plumes: 1. Waves, mean currents, and low-frequency

eddies. *J. Geophys. Res.,* **116,** C11027, doi:10.1029/2011JC007210.

Feng, Z., A. Reniers, B. K. Haus, and H. M. Solo-Gabriele, 2013: Modeling sediment-related enterococci loading, transport, and inactivation at an embayed nonpoint source beach. *Water Resour. Res.,* **49,** 693–712, doi:10.1029/2012WR012432.

Guza, R. T., and F. Feddersen, 2012: Effect of wave frequency and directional spread on shoreline runup. *Geophys. Res. Lett.,* **39,** L11607, doi:10.1029/2012GL051959.

Haile, R. W., and Coauthors, 1999: The health effects of swimming in ocean water contaminated by storm drain runoff. *Epidemiology,* **10,** 355–363.

Johnson, D., and C. Pattiaratchi, 2006: Boussinesq modelling of transient rip currents. *Coastal Eng.,* **53,** 419–439.

Kennedy, A. B., Q. H. Chen, J. T. Kirby, and R. A. Dalrymple, 2000: Boussinesq modeling of wave transformation, breaking and runup. I: One dimension. *J. Waterw. Port Coastal Ocean Eng.,* **126,** 39–47.

Kraichnan, R., and D. Montgomery, 1980: Two-dimensional turbulence. *Rep. Prog. Phys.,* **43,** 547–619, doi:10.1088/0034-4885/43/5/001.

Kuik, A. J., G. P. V. Vledder, and L. H. Holthuijsen, 1988: A method for the routine analysis of pitch-and-roll buoy wave data. *J. Phys. Oceanogr.,* **18,** 1020–1034.

Lippmann, T. C., T. H. C. Herbers, and E. B. Thornton, 1999: Gravity and shear wave contributions to nearshore infragravity motions. *J. Phys. Oceanogr.,* **29,** 231–239.

Long, J. W., and H. T. Özkan-Haller, 2009: Low-frequency characteristics of wave group–forced vortices. *J. Geophys. Res.,* **114,** C08004, doi:10.1029/2008JC004894.

Lumley, J. L., and E. A. Terray, 1983: Kinematics of turbulence convected by a random wave field. *J. Phys. Oceanogr.,* **13,** 2000–2007.

Lynett, P., 2006: Nearshore modeling using high-order boussinesq equations. *J. Waterw. Port Coastal Ocean Eng.,* **132,** 348–357.

Ma, G., F. Shi, and J. T. Kirby, 2011: A polydisperse two-fluid model for surfzone bubble simulation. *J. Geophys. Res.,* **116,** C05010, doi:10.1029/2010JC006667.

MacMahan, J. H., A. J. H. M. Reniers, and E. B. Thornton, 2010: Vortical surfzone velocity fluctuations with 0(10) min period. *J. Geophys. Res.,* **115,** C06007, doi:10.1029/2009JC005383.

Noyes, T. J., R. T. Guza, S. Elgar, and T. H. C. Herbers, 2002: Comparison of methods for estimating nearshore shear wave variance. *J. Atmos. Oceanic Technol.,* **19,** 136–143.

——, ——, ——, and ——, 2004: Field observations of shear waves in the surfzone. *J. Geophys. Res.,* **109,** C01031, doi:10.1029/2002JC001761.

——, ——, F. Feddersen, S. Elgar, and T. H. C. Herbers, 2005: Model-data comparisons of shear waves in the nearshore. *J. Geophys. Res.,* **110,** C05019, doi:10.1029/2004JC002541.

Nwogu, O., 1993: Alternative form of Boussinesq equations for nearshore wave propagation. *J. Waterw. Port Coastal Ocean Eng.,* **119,** 618–638.

Oltman-Shay, J., P. A. Howd, and W. A. Birkemeier, 1989: Shear instabilities of the mean longshore current: 2. Field observations. *J. Geophys. Res.,* **94** (C12), 18 031–18 042.

Özkan-Haller, H., and J. T. Kirby, 1999: Nonlinear evolution of shear instabilities of the longshore current: A comparison of observations and computations. *J. Geophys. Res.,* **104** (C11), 25 953–25 984.

Peregrine, D. H., 1998: Surf zone currents. *Theor. Comput. Fluid Dyn.,* **10,** 295–309.

Reniers, A. J. H. M., J. A. Roelvink, and E. B. Thornton, 2004: Morphodynamic modeling of an embayed beach under wave group forcing. *J. Geophys. Res.,* **109,** C01030, doi:10.1029/2002JC001586.

——, J. H. MacMahan, E. B. Thornton, and T. P. Stanton, 2007: Modeling of very low frequency motions during RIPEX. *J. Geophys. Res.,* **112,** C07013, doi:10.1029/2005JC003122.

——, ——, ——, ——, M. Henriquez, J. W. Brown, J. A. Brown, and E. Gallagher, 2009: Surf zone surface retention on a rip-channeled beach. *J. Geophys. Res.,* **114,** C10010, doi:10.1029/2008JC005153.

Rippy, M. A., P. J. S. Franks, F. Feddersen, R. T. Guza, and D. F. Moore, 2013: Factors controlling variability in nearshore fecal pollution: Fecal indicator bacteria as passive particles. *Mar. Pollut. Bull.,* **66,** 151–157, doi:10.1016/j.marpolbul.2012.09.030.

Rogers, J. S., S. G. Monismith, F. Feddersen, and C. Storlazzi, 2013: Hydrodynamics of spur and groove formations on a coral reef. *J. Geophys. Res. Oceans,* **118,** 3059–3073, doi:10.1002/jgrc.20225.

Ruessink, B. G., J. R. Miles, F. Feddersen, R. T. Guza, and S. Elgar, 2001: Modeling the alongshore current on barred beaches. *J. Geophys. Res.,* **106** (C10), 22 451–22 463.

Salmon, R., 1998: *Lectures On Geophysical Fluid Dynamics.* Oxford University Press, 378 pp.

——, 2002: Numerical solution of the two-layer shallow water equations with bottom topography. *J. Mar. Res.,* **60,** 605–638.

Slinn, D., J. Allen, P. Newberger, and R. Holman, 1998: Nonlinear shear instabilities of alongshore currents over barred beaches. *J. Geophys. Res.,* **103** (C9), 18 357–18 379.

Spydell, M. S., and F. Feddersen, 2009: Lagrangian drifter dispersion in the surfzone: Directionally spread, normally incident waves. *J. Phys. Oceanogr.,* **39,** 809–830.

——, and ——, 2012a: The effect of a non-zero Lagrangian timescale on bounded shear dispersion. *J. Fluid Mech.,* **691,** 69–94, doi:10.1017/jfm.2011.443.

——, and ——, 2012b: A Lagrangian stochastic model of surfzone drifter dispersion. *J. Geophys. Res.,* **117,** C03041, doi:10.1029/2011JC007701.

——, ——, R. T. Guza, and W. E. Schmidt, 2007: Observing surfzone dispersion with drifters. *J. Phys. Oceanogr.,* **37,** 2920–2939.

Sullivan, P. P., J. C. McWilliams, and W. K. Melville, 2007: Surface gravity wave effects in the oceanic boundary layer: Large-eddy simulation with vortex force and stochastic breakers. *J. Fluid Mech.,* **593,** 405–452, doi:10.1017/S002211200700897X.

Tabeling, P., 2002: Two-dimensional turbulence: A physicist approach. *Phys. Rep.,* **362,** 1–62, doi:10.1016/S0370-1573(01)00064-3.

Van Dongeren, A., A. Reniers, J. Battjes, and I. Svendsen, 2003: Numerical modeling of infragravity wave response during DELILAH. *J. Geophys. Res.,* **108,** 3288, doi:10.1029/2002JC001332.

Wei, G., J. T. Kirby, and A. Sinha, 1999: Generation of waves in Boussinesq models using a source function method. *Coastal Eng.,* **36,** 271–299.